# Validation of the Five-Phase Method for Simulating Complex Fenestration Systems with Radiance against Field Measurements

David Geisler-Moroder[1], Eleanor S. Lee[2], Gregory J. Ward[3]
[1]Bartenbach GmbH, Aldrans, Austria
[2]Lawrence Berkeley National Laboratory, Berkeley, CA, USA
[3]Anyhere Software, Albany, CA, USA

## Abstract

The Five-Phase Method (5-pm) for simulating complex fenestration systems with *Radiance* is validated against field measurements. The capability of the method to predict workplane illuminances, vertical sensor illuminances, and glare indices derived from captured and rendered high dynamic range (HDR) images is investigated. To be able to accurately represent the direct sun part of the daylight not only in sensor point simulations, but also in renderings of interior scenes, the 5-pm calculation procedure was extended. The validation shows that the 5-pm is superior to the Three-Phase Method for predicting horizontal and vertical illuminance sensor values as well as glare indices derived from rendered images. Even with input data from global and diffuse horizontal irradiance measurements only, daylight glare probability (DGP) values can be predicted within 10% error of measured values for most situations.

## Introduction

Over the past few years, tools and processes have been developed to accurately characterize and simulate the performance of optically complex daylighting and solar control systems in buildings. With the Radiance Three-Phase Method (3-pm), time-efficient annual daylight simulations of complex fenestration systems were enabled for the first time (Ward, 2007). The method was validated against field data by McNeil and Lee (2013).

An identified drawback of the 3-pm is the imprecise representation of the direct sun component through averaging over relatively large solid angles. As a result, significant errors can occur with certain types of systems, particularly in the assessment of visual discomfort. With the 5-pm, McNeil (2013) proposed an extension to the 3-pm to overcome this issue. Further algorithmic refinements were developed to increase the accuracy and resolution of input bidirectional scattering distribution function (BSDF) data. In this study, simulation results of the 5-pm with high-resolution BSDF input data were validated against field measurements for four daylighting systems.

## The Five-Phase-Method

The 3-pm allows efficient annual simulations by splitting up the daylight flux transfer from the sky to an interior surface or sensor point:

$$I = VTDS, \tag{1}$$

where $I$ is the resulting (il)luminance vector or matrix, $V$ is the view matrix that connects the sensor point with exiting directions of the façade system, T is the bidirectional transmission distribution function (BTDF) of the façade system, D is the daylight matrix that connects incident directions at the façade system with sky areas, and S is the discretized sky distribution vector or matrix.

The caveat is that the direct sun component is treated as part of the overall sky distribution and averaged over a large solid angle. The 5-pm improves that by removing the direct sun part from the 3-pm and substituting it with an improved calculation using the façade system's geometry or a high-resolution BSDF:

$$I = VTDS - V_dTD_dS_{ds} + C_{ds}S_{sun} \tag{2}$$

The 5-pm is explained in detail in (McNeil, 2013). This method works for illuminance sensors and luminances on interior room surfaces, but does not correctly represent the direct sun contribution to window luminance in renderings. To overcome this, we extend the calculation to:

$$I = VTDS - V_dTD_dS_{ds} + (C_{R\text{-}ds}+C_{F\text{-}ds})S_{sun} \tag{3}$$

The direct sun coefficient matrix $C_{ds}$ in (2) is thus replaced by the sum of two coefficient matrices for the direct sun part inside the room $C_{R\text{-}ds}$ and the direct sun part seen at the façade $C_{F\text{-}ds}$.

With *Radiance* the following simulation steps I) – VII) are performed for the overall 5-pm calculation for images. The additional generation of the transmission matrix T and the high-resolution BSDF representation of the façade system as used in the calculation of the matrices $C_{R\text{-}ds}$ and $C_{F\text{-}ds}$ are explained in section *"BSDF Characterization"*. The generation of the view matrix $V$ and daylight matrix $D$ as well as the sky descriptions $S$,


https://doi.org/10.26868/25222708.2017.401

$S_{ds}$, and $S_{sun}$ are explained in detail in (McNeil, 2010). Steps I and II are diagrammed here for completeness.

*I) Generate 3-pm view matrix V*

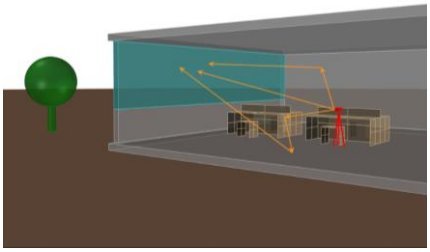

*Figure 1: Generation of view matrix V.*

*II) Generate 3-pm daylight matrix D*

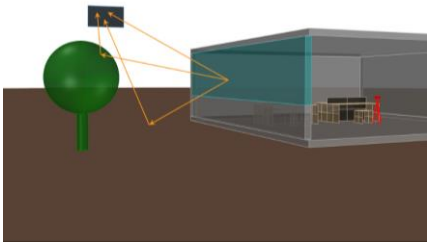

*Figure 2: Generation of daylight matrix D.*

*III) Generate direct only view matrix $V_d$*

In this step, the direct-only part of the view matrix is calculated. This includes all light from the window that reaches the camera or interior surfaces without interreflections. Because Radiance traces specular rays even when the interreflection calculation is turned off (-ab 0), a workaround is used to first compute illuminance renderings $V_{I\text{-}d}$ on ideal black surfaces and a material reflectance map $M_1$. As $V_{I\text{-}d}$ already contains luminances at the self-luminous diffuse plane representing the window, $M_1$ has to be set to 1 in this area. The illuminance renderings in the black scene are converted with the material reflectance map into the direct only view matrix $V_d$ (i.e. luminance images, which is possible for the Lambertian part of the reflectance as $L= E*\rho/\pi$):

$$V_d = V_{I\text{-}d} * M_1 \quad (4)$$

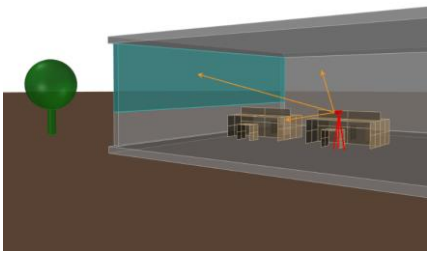

*Figure 3: Generation of material reflectance map $M_1$.*

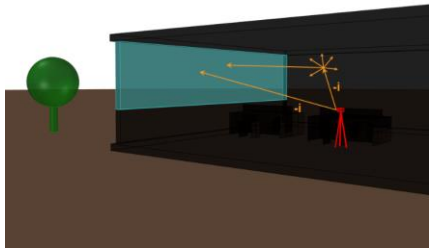

*Figure 4: Generation of illuminance renderings $V_{I\text{-}d}$ which are then converted into the direct only view matrix $V_d$ through the material reflectance map $M_1$.*

*IV) Generate direct only daylight matrix $D_d$*

Similar to $V_d$, all interreflections need to be excluded in the calculation of the direct light path from the sky to the outside (i.e., the incident plane) of the façade. Thus, all possible interacting surfaces again need to be set to an ideal absorber.

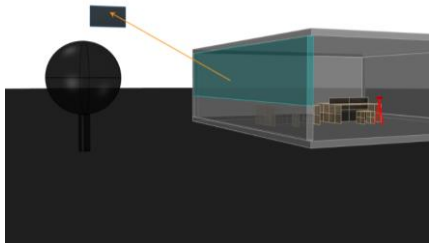

*Figure 5: Generation of direct only daylight matrix $D_d$.*

*V) Generate direct sun coefficient matrix for room surfaces $C_{R\text{-}ds}$*

To add back the direct part in higher detail, simulations with an improved representation of the façade (high-resolution BSDF or geometrical model) are performed. To allow for both improved results of the luminance patterns as seen at the façade itself and of the direct illumination on interior surfaces, the calculation has to be split up into two steps.

First, the direct sun room matrix $C_{R\text{-}ds}$ is generated similar as the direct only view matrix $V_d$ with two differences: the façade (i.e. the self-luminous interior side) is once replaced by a black material for the material reflectance map $M_2$ and once by a sophisticated transmitting model of the system for the illuminance renderings $C_{I\text{-}R\text{-}ds}$.

As for the direct only view matrix $V_d$ (eq. (4)), the illuminance images are converted through the material reflectance map $M_2$ into $C_{R\text{-}ds}$:

$$C_{R\text{-}ds} = C_{I\text{-}R\text{-}ds} * M_2 \quad (5)$$

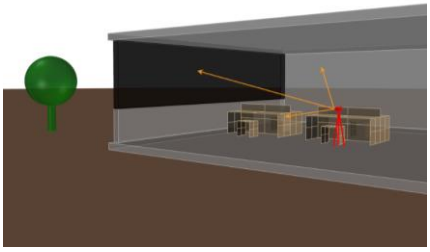

*Figure 6: Generation of material reflectance map $M_2$.*

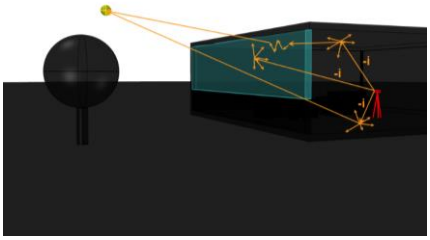

*Figure 7: Generation of illuminance renderings $C_{I\text{-}R\text{-}ds}$ which are converted into the direct sun coefficient room matrix $C_{R\text{-}ds}$ through the material reflectance map $M_2$.*

*VI) Generate direct sun coefficient matrix for the façade system $C_{F\text{-}ds}$*

To calculate an improved representation of the façade itself that includes the contribution of direct sun on and interreflected within the façade system itself, an additional rendering is performed in a model where the façade is represented by the high detail description (BSDF or geometry) and all other surfaces are set to black.

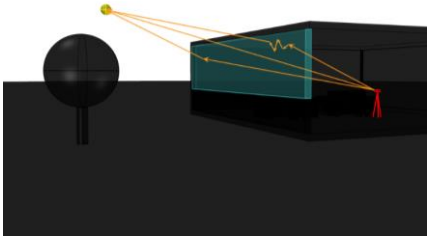

*Figure 8: Generation of direct sun coefficient façade matrix $C_{F\text{-}ds}$.*

*VII) Perform the matrix operations as given in eq. (3)*

According to eq. (3) the resulting images are combined to obtain the final 5-pm rendered image. In an example with the DL-L2 system in the upper section and venetian blinds lowered to block direct sunlight in the lower section (see section *"Field Measurements"*), Figure 9 shows the 3-pm result, the 3-pm direct-only part which is subtracted, and the 5-pm direct-only part which is added again.

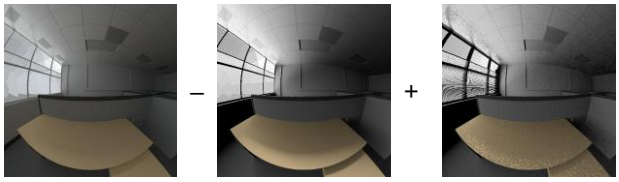

*Figure 9:3-pm result VTDS (left); 3-pm direct-only part $V_dTD_dS_{ds}$ (center); detailed 5-pm direct-only part, $(C_{R\text{-}ds}+C_{F\text{-}ds})S_{sun}$ (right).*

Figure 10 shows the resulting 5-pm image (right) compared to the 3-pm result (left). For both results the electric light was added to the final image. The main improvement is in the representation of the direct sun part that is seen in the upper section of the façade. Here the sun contribution is not spread out into a large solid angle, but represented as a small solar source. Though introducing some noise through the usage of a high-resolution BSDF combined with a limited number of ambient samples, the redirected component also shows sharper edges in the 5-pm result. The direct view of the blinds in the lower section is dominated by the indirect part, but still the structure of the single slats can clearly be seen in the 5-pm image.

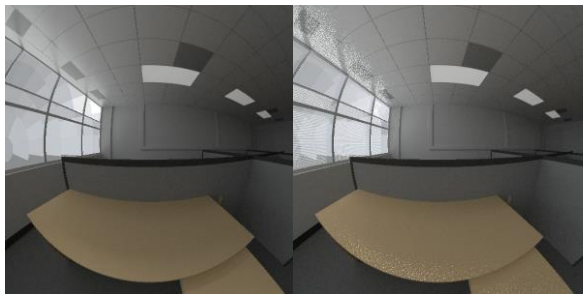

*Figure 10: Results with electric lighting added, 3-pm (left) and 5-pm (right).*

## Field Measurements

Full-scale field tests were conducted in the Lawrence Berkeley National Laboratory's new Facility for Low Energy Experiments in Buildings (FLEXLAB), Berkeley, California (37.87°N, 122.26°W). Two adjacent 6.1 m wide by 9.1 m deep by 2.7 m high south-facing test rooms were configured with the same interior finishes and low-height workstations to emulate open plan perimeter offices. A 6.1 m wide by 1.8 m high, dual-pane, low-emittance window was used in both rooms (Tv=0.64).

*Figure 11: Indoor photograph of the FLEXLAB test room.*

Several indoor and outdoor shading and daylighting systems were evaluated. The shade in the reference room was a 2.54-cm wide, indoor horizontal venetian blind lowered over the entire window with a fixed slat angle set to block direct sunlight. Three alternate systems were tested sequentially in the test room (further details in Lee et al. 2016):

a) *DL-L1*: a 1-mm thick daylighting film (Lucent Optics) with embedded microscopic reflectors designed to reflect light with maximum efficiency for profile angles between 45-65° (the remaining light is transmitted specularly);
b) *DL-L2*: a 375-micron thick daylighting film (SerraGlaze) with micro-replicated prisms designed to redirect sunlight with maximum efficiency for profile angles between 42-55° (for angles lower than 42° sunlight is transmitted specularly); and,
c) *S-L*: a light-weight solar screen (SmartLouvre Technology Ltd, MicroLouvre) consisting of 1.25-mm wide, 0.22 mm thick, matte black horizontal slats spaced vertically to produce a cut-off angle of 40°.

The first two daylight-redirecting films were installed indoors in the upper 0.6 m clerestory portion of the window with an indoor venetian blind in the lower 1.2 m vision portion of the window (similar to the reference room). The third solar screen was installed outdoors against the face of the window frame and covered the entire window (with no indoor blind).

Recessed fluorescent and LED fixtures were used in the reference and test rooms, respectively. The lights were set to a fixed output level so that the average workplane illuminance was approximately 300 lux. Total illuminance was monitored at various distances from the window at workplane height (Li-Cor LI-210SA, ± 3 lux, 1 scan/s, 1-min average). Daylight illuminance levels were determined by subtracting the electric light contribution from the total illuminance.

Field-of-view luminance and vertical illuminance were measured at various depths and viewpoints within each space using a digital camera (Canon EOS 5D; Sigma 4.5 mm fisheye lens). Figure 12 shows the resulting image for a typical user perspective in an office space. Low dynamic range (LDR) images were taken at 5-min intervals. Vertical illuminance was measured adjacent to each camera's lens, immediately before and after the bracketed set of LDR images, then used in the *hdrgen* compositing process to convert pixel data to photometric HDR data.

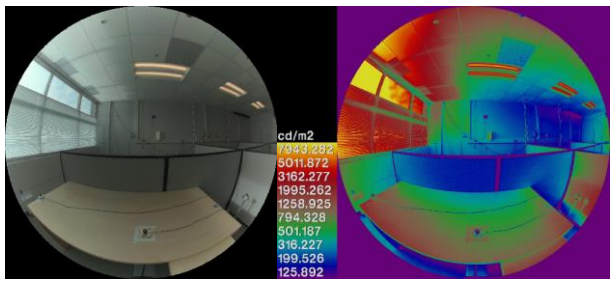


*Figure 12: Distortion-corrected equi-angular fisheye image representing a user's perspective in the office mockup with venetian blinds and a daylight redirecting system (left), luminance distribution (right).*

The *evalglare* tool (Wienold, 2012) was used to compute daylight glare probability (DGP). HDR images were first reduced to 799x799 pixels (*pfilt* -x /4.31 -y /4.31) prior to use in *evalglare*. Glare sources with a solid angle greater than 0.002 steradians (st) were identified in each image by *evalglare* using the default method: pixels with a luminance greater than the threshold luminance were identified as a potential glare source. The threshold luminance was defined as five times the average luminance within the entire 180° field of view or scene. Glare source pixels were then merged to one glare source given a search radius between pixels of 0.2 st. Non-glare source pixels were included with glare sources if they were surrounded by a glare source (i.e., smoothing option was used). Luminance peaks (>50,000 cd/m$^2$) were extracted as separate glare sources.

Global and diffuse horizontal irradiance were measured using instrumentation situated on the roof of the FLEXLAB facility (Delta-T Devices, SPN1, 0-2000 W/m$^2$, ± 8%, 1-min average). The validation dataset consisted of a full week of monitored data for each of the three systems around the equinox period.

## BSDF Characterization

Samples of the daylighting films were adhered to a 3-mm, clear glass substrate then measured at 81 incident angles (assuming right-left symmetry) using a scanning goniophotometer (pgII, pab Ltd) with adaptive sampling algorithms to capture more detailed data in areas where peak transmission occurred. Similar measurements were made of the solar screen, also at 81 incident angles.

These data were resampled to high-resolution tensor tree BSDFs using an interpolation method based on radial basis functions (Ward et al., 2014). Thus, the spatial

transmission properties of the façade components were reproduced at high detail, which is necessary to realistically simulate luminance values.

### BSDF interpolation

The techniques we developed to interpolate Bidirectional Scattering Distribution Function (BSDF) measurements are described in broad terms in (Ward et al., 2014) and in greater detail in (Ward et al., 2012). The essential problem is to fill in missing/unmeasured information to complete an arbitrary 4-dimensional (i.e., anisotropic) BSDF and represent it in a form that can be used efficiently in physically-based rendering and simulation.

We acknowledge that it is impractical to measure all the incident and scattered directions we might need for a given reflecting or transmitting material. In particular, daylight redirecting systems tend to be anisotropic (not rotationally symmetric) and fail to fit common mathematical models. However, they behave consistently enough that we can interpolate densely measured scattering distributions between sparsely measured incident directions.

An example measurement pattern for scattered and incident directions is shown in Figure 13. The scattered distribution (a) recorded by the pab Ltd pgII goniophotometer includes higher density sampling near the preferred scattering direction, but also shows gaps and holes due to the device geometry and source-detector interference. These areas need to be interpolated. The more challenging problem is how to interpolate smoothly between the relatively wide spacing of the measured incident directions shown in (b).

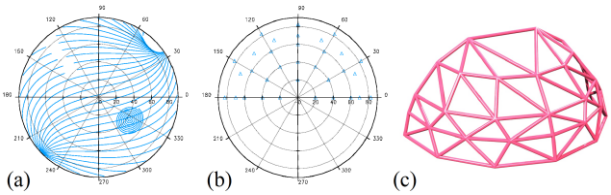


*Figure 13: (a) Scattering directions measured by pab Ltd pgII. (b) Selected incident directions for a BSDF with bilateral symmetry. (c) Incident directions organized into Delaunay mesh.*

Our interpolation proceeds in five stages:

1. Organize BSDF measurements into (partial) incident and scattered hemispheres.
2. For each incident direction, fit a Radial Basis System (RBS), which is a collection of Gaussian lobes, to the measured scattering data.
3. Sort the incident directions into a Delaunay triangle mesh (c) and calculate transport plans to get from each RBS scattering distribution to its nearest neighbor along each edge.
4. Deduce BSDF symmetry based on measured incident directions: isotropic (90° arc), quadrilateral (quarter hemisphere), bilateral (half hemisphere), or no symmetry (full hemisphere).
5. Collect incident and scattered hemispheres to interpolate the BSDF over all directions and represent it in a matrix or tensor tree data format useful for simulation and rendering.

Step 1 is simple and self-explanatory. Step 2 fits roughly 50-200 Gaussian lobes to the measured data. Each lobe has a central direction, a peak value, and a half-maximum distance (angle). The lobes should sum to a reasonable representation of the measured data, with some smoothing applied.

Step 3 calculates a *transport plan* along each Delaunay edge, which says how one RBS morphs into its neighbor. This is encoded in a coefficient matrix, where the number of rows corresponds to the source Gaussian lobes and the number of columns to the destination Gaussian lobes. Each coefficient in this sparse matrix indicates the amount of energy from one lobe that is conveyed to another lobe. This enables us to create any RBS we like along the edge by partial displacement as described in (Bonneel et al. 2011). We have extended this method to include points in the interior of each incident direction triangle by interpolating first across one edge then towards the opposite vertex.

Step 4 is a straightforward application of symmetry based on which incident angles the operator chose to measure. This selection is based in turn on the observed system symmetry. For example, a venetian blind system has clear bilateral symmetry. A prismatic device comprised of square pyramids would have quadrilateral symmetry. A piece of sand-blasted glass would be isotropic (rotational symmetry).

Finally, step 5 interpolates the BSDF representation in order to convert it to a more convenient form. While we could perform our simulations directly from the displaced RBS distributions, this is an expensive proposition compared to other, better optimized representations. In particular, we find it convenient to derive a matrix BSDF representation for annual calculations involving operable shading systems, allowing us to quickly swap complex fenestration systems or settings in a simulation depending on current daylight and occupant conditions. Where greater accuracy or angular resolution is needed, we prefer a tensor tree representation, which subdivides as needed around peaks in the distribution for more time- and space-efficient simulations.

Both the matrix and tensor tree representations are recorded in a standard eXtended Markup Language (XML) file and read in by a C library that supports BSDF queries and sampling operations. This library is employed by *Radiance* and other simulation tools that make use of the shared XML data.

## Simulations

The FLEXLAB was virtually rebuilt and simulated utilizing the 5-pm in *Radiance*.

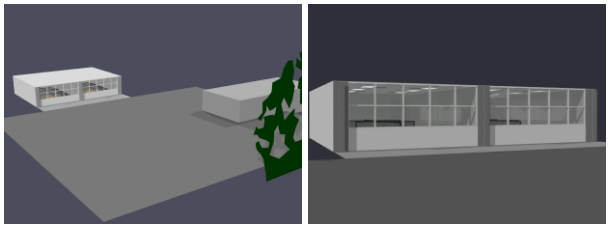

*Figure 14: Simulation model of LBNL's new Facility for Low Energy Experiments in Buildings (FLEXLAB).*

While the original 5-pm version as in eq. (2) could be used for the illuminance sensor calculations, for the luminance renderings we applied the extended method as stated above in eq. (3).

For the illuminance sensor points, simulations were performed and compared for daylight results without electric lighting (see also section *"Field Measurements"*). To compare glare evaluations between camera and rendered images, however, it is necessary to account for the additional sources of illumination as well. The electric lighting from the fluorescent and LED fixtures in the reference and test rooms were approximated as emitting luminous surfaces. The luminous intensity distribution as given in the luminaire's IES files was applied. Separate simulations were performed with electric lighting only. The resulting images were then added to the simulated daylighting situations to obtain the overall illumination.

The daylighting systems were characterized by BSDFs measured with a scanning goniophotometer and resampled to high-resolution tensor tree BSDFs using the interpolation method as described above. Thus, the spatial transmission properties of the façade components were reproduced at high detail, which was necessary to realistically simulate interior luminance values. Both, a Klems representation (145 directions) for the 3-pm calculations and a tensor tree representation (option-*t4 7* for a maximum resolution of 1.4°) for the advanced direct sun calculations were created.

BSDFs for the venetian blinds in the reference room were generated with *genBSDF* using a geometrical model of the shading system and a measured reflectance value (ρ = 0.733). Again, a Klems representation for the 3-pm calculations and a tensor tree representation (*-t4 6* for a maximum resolution of 2.8°) for the advanced direct sun calculations were derived.

The measured global and diffuse horizontal irradiance values were used as input to the simulations. The direct horizontal irradiance (difference between global and diffuse) was converted to direct normal irradiances using hourly sun positions. Together with the diffuse horizontal irradiances a climate data file in the *Daysim* format with values for every 5 minutes was generated. Using the *Radiance* tool *gendaymtx* this climate data was then transformed into discretized Perez sky representations $S$, $S_{ds}$ and $S_{sun}$ (the necessary input to eq. (3)).

## Results

The simulations were performed for the weekly periods with the different systems installed. All sensor values and images were simulated in 5 minute intervals, i.e. 1728 time steps for the 6-day periods (systems DL-L1 and S-L) and 2016 time steps for the 7-day period (system DL-L2). The evaluations were performed for the times between 9am and 5pm representing working hours with adequate daylight provision. The main interest is to show that the 5-pm is adequate to perform glare evaluations. Thus, the calculations in this validation work were focused on vertical illuminance and image-based metrics. Validation of workplane illuminance provided additional proof that the 5-pm is adequate.

### Workplane illuminances

Figure 15 shows an example day comparing horizontal illuminance measurements (on the desk near the façade, close to the position of the vertical illuminance sensor and the evaluated camera, see below) compared to simulation results from the 3-pm and the 5-pm, respectively, for the test room with the DL-L2 system.

Table 1 shows for the test room set-ups and the reference rooms with venetian blinds (VB) that the 5-pm is even better able to predict interior illuminance values. The slightly lower match between measurement and simulation with the 5-pm than with the 3-pm for the system S-L leads to the assumption that there are some artefacts in the measured BSDF data. This needs to be further evaluated (see section on future work).

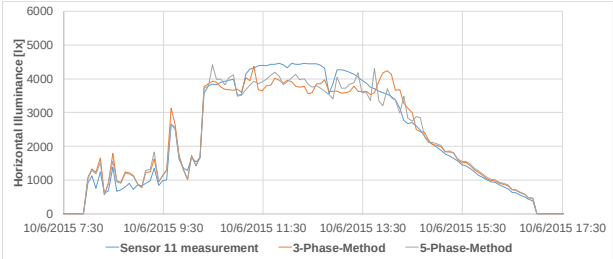


*Figure 15: Comparison of horizontal illuminances in the test room (DL-L2 in upper section, venetian blinds in lower section of the façade) on October 6th.*

*Table 1: Frequency (% of measured period) of deviations in horizontal illuminance between simulation results and measurements (Δ%) for sensor on desk close to façade.*

| | 3-Phase Method | | | 5-PhaseMethod | | |
|---|---|---|---|---|---|---|
| Set-Up | Δ < 5% | Δ < 10% | Δ < 20% | Δ < 5% | Δ < 10% | Δ < 20% |
| DL-L1 | 16.8% | 33.5% | 58.3% | 29.0% | 53.9% | 85.0% |
| Ref VB | 15.7% | 42.7% | 94.9% | 31.9% | 73.0% | 94.3% |
| DL-L2 | 26.7% | 55.2% | 86.9% | 28.2% | 61.3% | 92.9% |
| Ref VB | 17.9% | 46.9% | 95.1% | 44.5% | 85.7% | 94.5% |
| S-L | 28.2% | 55.1% | 78.7% | 25.0% | 50.9% | 74.1% |
| Ref VB | 22.7% | 49.4% | 88.1% | 35.2% | 70.2% | 88.3% |

### Vertical illuminances at eye

Vertical illuminances were captured in the field measurements at the three positions: facing the façade from the front and the back of the room, and parallel to the façade mimicking a view position at the workplace near the window. Figures 16 to 18 show example results for measurements compared to simulation results from the 3-pm and the 5-pm, respectively, for various days and façade systems.

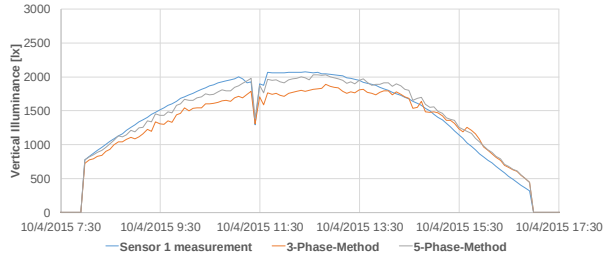


*Figure 16: Comparison of vertical illuminances in the reference room (venetian blinds in both sections of the façade) on October 4th.*

Although the venetian blind slats are positioned to block direct sunlight, the coarse Klems representation used in the 3-pm is inferior to the geometric representation used in the 5-pm (Figure 16). This behavior is even more pronounced in Figures 17 and 18 where the 3-pm predicts a strong peak where there is none.

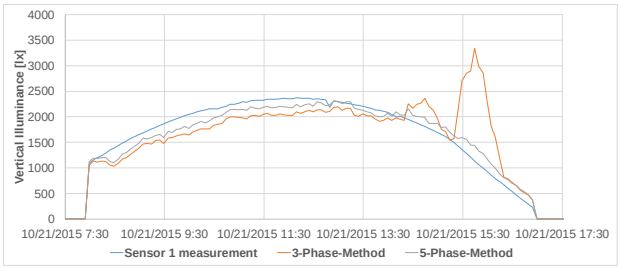


*Figure 17: Comparison of vertical illuminances in the reference room (venetian blinds in both sections of the façade) on October 21st.*

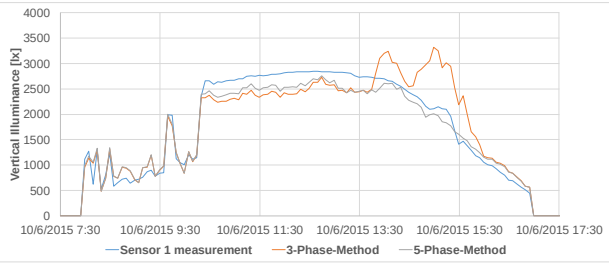


*Figure 18: Comparison of vertical illuminances in the test room (DL-L2 in upper section, venetian blinds in lower section of the façade) on October 6th.*

Table 2 shows the frequency of deviations between the simulated and the measured values. Generally, the 5-pm outperforms the 3-pm in terms of prediction of (vertical) illuminances. For the DL-L2 system above 75% of the values could be predicted within 10% accuracy, and more than 96% within 20% accuracy. We could reach similar results for the reference situations to DL-L1 and DL-L2. For DL-L1 only 52% matched within 10%, but again 92% showed deviations below 20%. As already seen for horizontal illuminances, the results for the S-L system show slightly higher deviations for the 5-pm than for the 3-pm. The assumed discrepancies due to the measured BSDF data will be further analyzed.

*Table 2: Frequency of deviations in vertical illuminance between simulation results and measurements.*

| | 3-Phase Method | | | 5-PhaseMethod | | |
|---|---|---|---|---|---|---|
| Set-Up | Δ < 5% | Δ < 10% | Δ < 20% | Δ < 5% | Δ < 10% | Δ < 20% |
| DL-L1 | 16.3% | 35.6% | 75.9% | 20.6% | 52.1% | 92.0% |
| Ref VB | 14.8% | 30.8% | 81.2% | 40.0% | 74.0% | 87.5% |
| DL-L2 | 18.2% | 47.0% | 89.4% | 33.1% | 75.5% | 96.3% |
| Ref VB | 22.0% | 45.5% | 89.7% | 49.8% | 77.9% | 90.9% |
| S-L | 22.7% | 45.2% | 67.7% | 21.9% | 41.0% | 65.1% |
| Ref VB | 14.2% | 29.5% | 72.8% | 23.6% | 54.9% | 75.8% |

### Glare evaluations

Images were captured at the same three positions as the vertical illuminance measurements. For the glare evaluations the position mimicking a user's view at the workplace near the façade is used (see Figure 19).

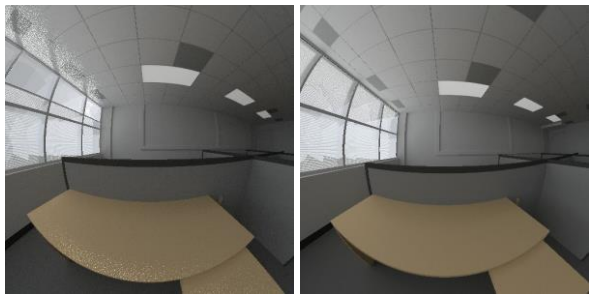

*Figure 19: 5-pm rendering results for a typical user perspective used for glare evaluations in test room (left) and reference room (right).*

Figures 20 to 23 show example results for DGP results calculated from captured photographs compared to 3-pm and 5-pm simulation results for various days and façade systems.

The results for the DGP evaluations are comparable to the vertical illuminance results. As the DGP is mainly influenced by the vertical illuminance – especially for scenes without pronounced bright spots such as direct sunlight – this is also expected in the investigated scenes where the venetian blinds were set to block the direct sun beam. Again, the 3-pm overestimates glare in the afternoon, which is due to averaging the direct solar component into a large solid angle and thus transmitting it through the venetian blinds.

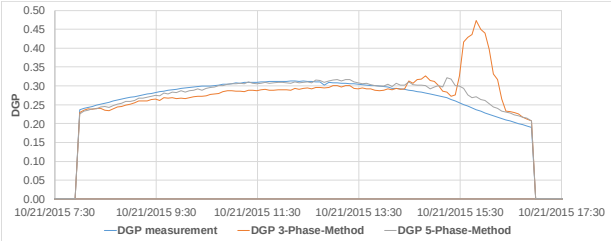


*Figure 20: Comparison of DGP values in the reference room (venetian blinds in both sections of the façade) on October 21st.*

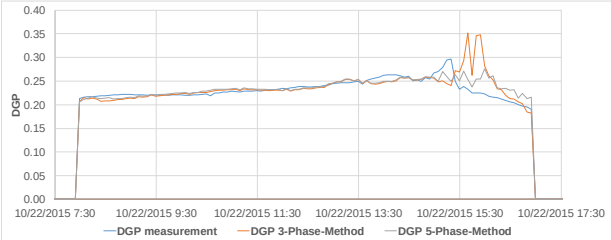


*Figure 21: Comparison of DGP values in the test room (S-L in upper section, venetian blinds in lower section of the façade) on October 22nd.*

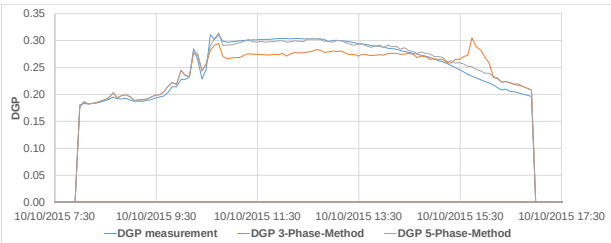


*Figure 22: Comparison of DGP values in the reference room (venetian blinds in both sections of the façade) on October 10th.*

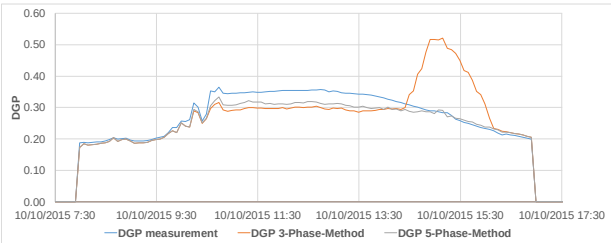


*Figure 23: Comparison of DGP values in the test room (DL-L1 in upper section, venetian blinds in lower section of the façade) on October 10th.*

Table 3 shows the frequency of deviations between the simulated and the measured values. Again, the 5-pm outperforms the 3-pm in terms of DGP calculations. For the reference situations with venetian blinds more than 68% of the DGP values could be calculated with a deviation of less than 5% and most could be predicted with errors below 10%. The test room situations with daylighting systems installed could still be reproduced with less than 10% deviation for most scenes.

*Table 3: Frequency of deviations between simulated DGP values and results calculated from photographs.*

| | 3-Phase Method | | | 5-PhaseMethod | | |
|---|---|---|---|---|---|---|
| Set-Up | Δ < 5% | Δ < 10% | Δ < 20% | Δ < 5% | Δ < 10% | Δ < 20% |
| DL-L1 | 16.7% | 32.7% | 84.4% | 36.6% | 74.5% | 99.7% |
| Ref VB | 39.2% | 91.7% | 97.1% | 76.5% | 97.5% | 100% |
| DL-L2 | 23.9% | 75.9% | 94.2% | 62.7% | 94.8% | 99.4% |
| Ref VB | 60.2% | 99.2% | 100% | 76.7% | 100% | 100% |
| S-L | 83.8% | 93.1% | 97.7% | 82.4% | 93.1% | 98.1% |
| Ref VB | 29.8% | 80.6% | 90.6% | 68.0% | 81.8% | 97.6% |

Glare evaluations were also done according to the DGI metric. Figure 24 shows the DGI values calculated from the photographs and the 3-pm and 5-pm simulations for an example day.

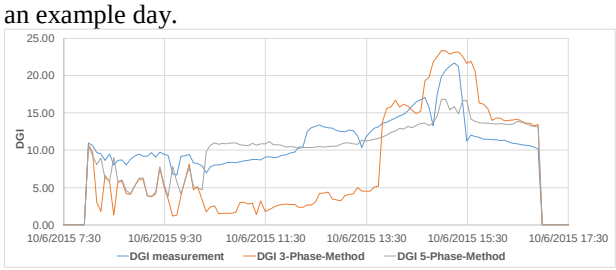


*Figure 24: Comparison of DGI values in the test room (DL-L2 in upper section, venetian blinds in lower section of the façade) on October 6th.*

Table 4 shows the frequency of deviations between the simulated and the measured DGI values. The 5-pm outperforms the 3-pm in most situations, but the general match is much lower than for DGP values. As the DGI calculation does not take the vertical illuminance into account, variations in luminances are directly influencing the results.

*Table 4: Frequency of deviations between simulated DGI values and results calculated from photographs.*

| | 3-Phase Method | | | 5-PhaseMethod | | |
|---|---|---|---|---|---|---|
| Set-Up | Δ < 5% | Δ < 10% | Δ < 20% | Δ < 5% | Δ < 10% | Δ < 20% |
| DL-L1 | 3.9% | 6.6% | 11.3% | 14.7% | 28.7% | 48.5% |
| Ref VB | 16.5% | 30.9% | 56.2% | 14.8% | 25.2% | 68.7% |
| DL-L2 | 4.1% | 10.3% | 18.3% | 8.6% | 16.5% | 53.9% |
| Ref VB | 21.3% | 41.8% | 75.8% | 15.9% | 32.6% | 72.4% |
| S-L | 37.7% | 56.5% | 78.2% | 36.1% | 56.6% | 78.2% |
| Ref VB | 9.2% | 15.7% | 33.9% | 16.5% | 36.3% | 64.6% |

## Conclusion

The Five-Phase Method (5-pm) for simulation of complex fenestration systems with *Radiance* was validated against field measurements in terms of workplane illuminances, vertical illuminances and glare evaluations. The 5-pm was extended to accurately represent the direct sun part of the daylight also in renderings of interior scenes. Measurements were performed in LBNL's new Facility for Low Energy Experiments in Buildings for four different daylight systems. The system transmission properties of the daylight systems were measured using a pab Ltd pgII goniophotometer and transformed into BSDF datasets for use in simulations using a newly developed

interpolation technique. The reference venetian blinds were characterized through simulated BSDFs. The weather data input was based on measured global and diffuse horizontal irradiances only.

Summarizing, the 5-pm clearly outperforms the Three-Phase Method for predicting horizontal and vertical illuminance sensor values as well as glare metrics derived from rendered images. For all metrics and all investigated systems, the 5-pm results show lower deviations from the values obtained with field measurement. Even with input from global and diffuse horizontal irradiance data only, DGP values could be predicted to within 10% error for most situations.

Reasons for remaining deviations between the 5-pm simulations and the measurement values are manifold: For example, the exterior irradiance measurement input data is transformed into a sky description using the Perez model, which – for single situations – might differ significantly from the real sky conditions. The venetian blind reference system was geometrically modeled to derive BSDF data. However, the same exact positioning and settings of tilt angles cannot be guaranteed in reality.

## Future Work

The validation work should be extended to cover additional phenomena. Data from a winter and summer measurement period should be used to evaluate the performance for other direct sunlight incident angles. Using more detailed input data such as measured sky luminances from an HDR imaging system (Terrestrial Light, 2016) is expected to further increase the goodness of fit for the 5-pm simulation results. Scenes where direct sunlight hits the interior space may demonstrate the benefits of the 5-pm over the 3-pm even more. This would also lead to more times where the glare indices are in a critical range. Additionally, the effects of variations in the parameters used in the BSDF interpolation routine, especially the smoothing factor, should be investigated and deviations as seen for the system *S-L* analyzed. An updated tutorial for the extended Five-Phase Method is underway and will be publicly available.

## Acknowledgement

This work was supported by the Assistant Secretary for Energy Efficiency and Renewable Energy, Building Technologies Program, of the U.S. Department of Energy, under Contract No. DE-AC02-05CH11231, by the California Energy Commission through its Electric Program Investment Charge (EPIC) Program on behalf of the citizens of California, by Pacific Gas and Electric Company's Emerging Technologies Program, and by the Austrian Research Promotion Agency (FFG) through the "lightSIMheat" project under Contract No. 838718.

## References

Bonneel, N. et al. (2011). Displacement interpolatuion using Lagrangian mass transport, ACM TOG 30, 6, 158:1-158:12. (Proc. SIGGRAPH Asia '11).

Lee, E.S. et al. (2016). Technology Assessments of High Performance Envelope with Optimized Lighting, Solar Control, and Daylighting. Pacific Gas and Electric Company's Emerging Technologies Program, ET Project Number: ET14PGE8571.

McNeil, A. (2010). The Three-Phase Method for Simulating Complex Fenestration with Radiance.www.radiance-online.org/learning/tutorials/ Tutorial-ThreePhaseMethod.pdf

McNeil, A. (2013). The Five-Phase Method for Simulating Complex Fenestration with Radiance. http://radiance-online.org/learning/tutorials/fivephasetutorialfiles/Tutorial-FivePhaseMethod_v2.pdf, 1-23.

McNeil, A., Lee, E.S. (2013). A validation of the Radiance three-phase simulation method for modelling annual daylight performance of optically complex fenestration systems. J Building Performance Simulation 6(1), 24-37.

Terrestrial Light (2016). Skyometer. Online: http://terrestriallight.com

Ward, G. (2007). Utilizing BTDF Window Data, 6th Intl. Radiance Workshop, Minneapolis, MN, USA, October 2007.

Ward, G., Kurt, M., Bonneel, N. (2012). A Practical Framework for Sharing and Rendering Real-World Bidirectional Scattering Distribution Functions. October 2012. LBNL-5954E. online: http://eetd.lbl.gov/node/51625.

Ward, G. et al. (2014). Reducing Anisotropic BSDF Measurement to Common Practice. Proceedings of the Eurographics 2014 Workshop on Material Appearance Modeling.

Wienold J. (2012). *Evalglare*, version 1.0, Fraunhofer Institute for Solar Energy Systems, Freiburg, Germany.